Multisubband photoluminescence in sawtooth doping superlattices

E. F. Schubert and T. D. Harris
AT&T Bell Laboratories, Murray Hill, New Jersey 07974

J. E. Cunningham and W. Jan
AT&T Bell Laboratories, Holmdel, New Jersey 07733
(Received 29 December 1988)

Photoluminescence spectra on doping superlattices consist of multiple, clearly resolved, interband transitions between quantum-confined states. Not only the ground-state transition is observed, but also higher-energy transitions due to an opposite energy dependence of the oscillator strength and thermal distribution of carriers. Variational solutions of the three lowest states are used to obtain consistent understanding of optical emission spectra in sawtooth doping superlattices. Under higher excitation intensities, the photoluminescence peak energies of the quantum-confined transitions shift to higher energies, and new transitions become observable. The changes of the photoluminescence spectra can be understood on the basis of screening, band filling, and increased carrier temperature at higher excitation intensity.

The physical properties of microstructured semiconductors are of remarkable interest, since they are the only branch of physics that enables tailoring and fabrication of potentials in the quantum regime. Square-shaped and parabolic potential wells have been emphasized,[1,2] and significant progress in recent years has emerged. The quantum-mechanical potentials can be generated by abrupt changes in composition of a semiconductor, for example in the system $Al_xGa_{1-x}As/GaAs$. In addition, variation of dopant concentration also results in quantum-mechanical potentials, as proposed by Esaki and Tsu.[3] The largest potential modulation is obtained by employing a doping profile represented by a train of delta functions alternating in n- and p-type dopants.[4,5] The band-edge potentials can then become sawtooth shaped. Recently, we have demonstrated quantum-confined absorption in such a sawtooth superlattice.[5]

In this paper we report on photoluminescence spectroscopy of GaAs sawtooth superlattices. Multisubband luminescence is observed and clearly resolved for the first time in a doping superlattice. Interband transition energies are compared with energies of a variational calculation. It will be shown that the oscillator strength and thermal distribution of carriers have opposite dependences on energy: while the thermal population decreases exponentially with energy, the oscillator strength increases exponentially with the quantum number. The unique interplay of thermal population, oscillator strength, and state density, which is not found in other structures, allows us to simultaneously observe optical transitions of comparable intensity between different quantum-confined states of the superlattice. Photoluminescence peaks shift to higher energies at increased excitation intensity. Furthermore, high-energy subband transitions gain in relative intensity and new high-energy quantum-confined transitions become observable at increased excitation intensity.

The doping profile of the superlattice can be represented by a train of alternating n-type and p-type δ functions:

$$N(z)=N_D^{2D}\sum_i \delta(z-iz_p)-N_A^{2D}\sum_i \delta(z-(\tfrac{1}{2}+i)z_p)\ , \tag{1}$$

where $N^{2D}=N_D^{2D}=N_A^{2D}$ are the two-dimensional donor and acceptor concentrations, and z_p is the period of the superlattice. A thin doping profile results in an electric field of magnitude

$$F=eN^{2D}/2\epsilon\ , \tag{2}$$

where e is the elementary charge, and ϵ is the permittivity of the semiconductor. Consequently, the potential energy of a one-dimensional V-shaped potential well is given by $U(z)=eFz$ for $z\geq 0$, and $U(z)=-eFz$ for $z<0$.

The solution of the Schrödinger equation using a variational method provides eigenstate energies and wave functions with a particularly simple analytical form. The trial functions used for the lowest three states are

$$\psi_0(z)=A_0(1+\alpha_0 z)e^{-\alpha_0 z} \quad \text{for } z\geq 0\ , \tag{3a}$$

$$\psi_0(z)=A_0(1-\alpha_0 z)e^{\alpha_0 z} \quad \text{for } z<0\ , \tag{3b}$$

$$\psi_1(z)=A_1 z e^{-\alpha_1 z} \quad \text{for } z\geq 0\ , \tag{4a}$$

$$\psi_1(z)=A_1 z e^{\alpha_1 z} \quad \text{for } z<0\ , \tag{4b}$$

$$\psi_2(z)=A_2(\alpha_2^2 z^2-1)(1+\alpha_2 z)e^{-\alpha_2 z} \quad \text{for } z\geq 0\ , \tag{5a}$$

$$\psi_2(z)=A_2(\alpha_2^2 z^2-1)(1-\alpha_2 z)e^{\alpha_2 z} \quad \text{for } z<0\ . \tag{5b}$$

These trial functions use the fact that ψ_0 and ψ_2 have even spatial symmetry, while ψ_1 is an odd function. The wave function $\psi_1(z)$ is identical to the Fang-Howard wave function[6] for positive z. The normalization condi-

tion $\langle \psi_n | \psi_n \rangle = 1$ yields the parameters A_n, with

$$A_0^2 = \tfrac{2}{5}\alpha_0, \quad A_1^2 = 2\alpha_1^3, \quad A_2^2 = \tfrac{4}{63}\alpha_2 . \tag{6}$$

Minimization of the energy expectation values yields the trial parameters α_n:

$$\begin{aligned} \alpha_0 &= (\tfrac{9}{4})^{1/3}(eF2m^*/\hbar^2)^{1/3} , \\ \alpha_1 &= (\tfrac{3}{4})^{1/3}(eF2m^*/\hbar^2)^{1/3} , \\ \alpha_2 &= (\tfrac{47}{12})^{1/3}(eF2m^*/\hbar^2)^{1/3} , \end{aligned} \tag{7}$$

and finally the energies

$$E_0 = \frac{3}{10}\left[\frac{9^2}{2}\right]^{1/3}\left[\frac{e^2\hbar^2F^2}{2m^*}\right]^{1/3} , \tag{8a}$$

$$E_1 = \frac{3}{2}\left[\frac{9}{2}\right]^{1/3}\left[\frac{e^2\hbar^2F^2}{2m^*}\right]^{1/3} , \tag{8b}$$

$$E_2 = \frac{9}{7}\left[\frac{47}{12}\right]^{2/3}\left[\frac{e^2\hbar^2F^2}{2m^*}\right]^{1/3} . \tag{8c}$$

These energies are in very good agreement (better than 2%) with the exact solution of the V-shaped potential well using Airy functions.[5]

We now proceed to calculate the overlap integral to evaluate the dependence of the oscillator strength on the transition energy between the quantum states. The matrix element of a quantum-confined transition in a sawtooth superlattice involves mostly the exponentially decaying part of the wave functions, as shown in Fig. 1. In a first-order approach, we assume $\alpha \cong \alpha_1 \cong \alpha_2 \cong \alpha_3$.[7] The limits of the integration are chosen in such a way that integration is limited to the region beyond the classical turning points z_{it} and z_{ft} of the initial (electron) and final (hole) state, as shown in Fig. 1. Evaluation of the overlap integral yields

$$\int_{z_{ft}}^{z_p/2-z_{it}} \psi_i(z)\psi_f(z)dz \cong \frac{\psi_i(z_{it})\psi_f(z_{ft})}{\alpha_f - \alpha_i} e^{-\alpha_i(z_p/2 - z_{it} - z_{ft})} . \tag{9}$$

For the calculation of this result we use the fact that the electron mass is lighter than either heavy- or light-hole mass, i.e., $\alpha_i < \alpha_f$. Since the turning points depend on the eigenstate energies according to $z_{it} = E_i/eF$ and $z_{ft} = E_f/eF$, it is evident that the oscillator strength depends exponentially on the eigenstate energy due to an increasing overlap of wave functions. Finally, we point out that *all* transitions are allowed in the sawtooth structure.[5]

The epitaxial GaAs superlattices are grown by gas-source molecular-beam epitaxy on semi-insulating substrates at a low temperature of $\leq 550\,^{\circ}\mathrm{C}$ to keep diffusion minimal. The nominal doping concentration is $N^{2D} \cong N_D^{2D} \cong N_A^{2D} = 1.25 \times 10^{13}$ cm^{-2}, and the period is $z_p = 150$ Å. Low-temperature photoluminescence measurements are performed with the samples immersed into superfluid He. The 488-nm line of an Ar^+-ion laser and the 647-nm line of a Kr^+-ion laser are used for excitation. The excitation intensity was varied using neutral-density filters. The photogenerated carrier density is estimated to be in the 10^{17}-cm^{-3} range. Luminescence is detected with a Ge-pin detector cooled to 77 K.

Figure 2 shows the low-temperature photoluminescence spectrum of the sawtooth superlattice. Three clearly resolved photoluminescence peaks are observed at $\lambda \cong 0.98$, 1.02, and 1.09 μm. Furthermore, a shoulder is observed at the high-energy side of the spectrum at $\lambda \cong 0.95$ μm. We attribute the clearly resolved luminescence peaks to transitions between quantum-confined conduction- and valence-band states. The assignment of luminescence peaks is confirmed by calculation of transition energies and comparison with experimentally observed peak energies. A very good fit between experimental and calculated peak energies is obtained by using $N^{2D} = 1.3 \times 10^{13}$ cm^{-2} and $z_p = 142$ Å. Five transitions can be identified, namely the $0e \rightarrow 0hh$, $0e \rightarrow 0lh$, $0e \rightarrow 1hh$, $0e \rightarrow 2hh$, and $1e \rightarrow 0hh$ transitions.

Most strikingly, however, the photoluminescence spectrum of Fig. 2 displays not only the *lowest* transition but also transitions via excited states, e.g., the $0e \rightarrow 1hh$ transition. Furthermore, excited-state transitions (e.g., $0e \rightarrow 0lh$ or $0e \rightarrow 1hh$ are more intense than the ground-state ($0e \rightarrow 0hh$) transition. The light-hole transition is stronger than the heavy-hole transition, even though the density of states of the light-hole subband is much smaller (approximately a factor of $m^*_{hh}/m^*_{lh} \cong 7$). Such photoluminescence spectra were hitherto not observed in any quantum-well structure. We will now show that the specific characteristics of the photoluminescence spectrum can be consistently explained in terms of the unique energy dependence of the oscillator strength of the sawtooth structure.[8]

For completeness, we note that multisubband transitions were observed in compositional quantum-well struc-

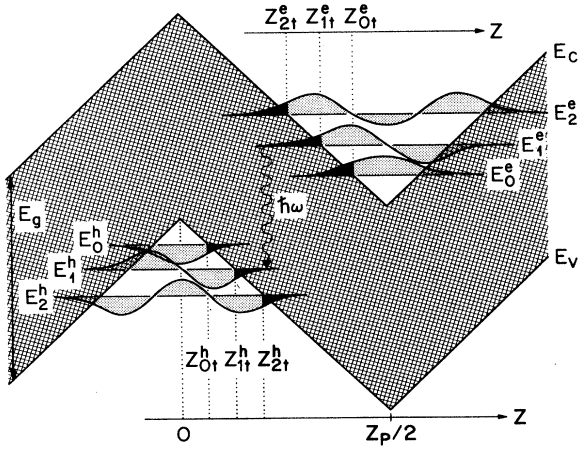

FIG. 1. Schematic illustration of the sawtooth superlattice band diagram. Overlap of electron and hole wave functions occurs in the classically forbidden region (cross-hatched), i.e., beyond the classical turning points.

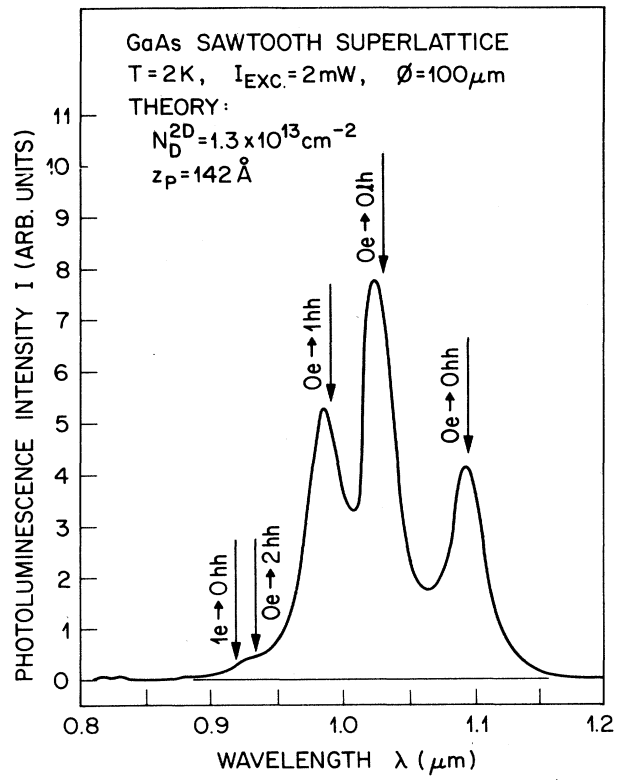

FIG. 2. Low-temperature photoluminescence spectrum of a sawtooth superlattice. The arrows indicate theoretical energies of quantum-confined transitions.

tures at very high excitation intensities.[9] However, the intensity of those transitions was found to decrease exponentially with energy.[9] Multisubband photoluminescences were not observed in conventional homogeneously doped *n-i-p-i* structures.[8]

The photoluminescence line shape in semiconductors and semiconductor quantum-well structure can usually be determined by the product of the joined density of states and the thermal distribution of carriers. The latter is usually modeled in terms of a Boltzmann distribution and a carrier temperature.[10] The carrier temperature depends on the photoluminescence excitation intensity and is typically in the range $10 \leq T_C \leq 50$ K at a lattice temperature of $T_l = 2$ K. The transition-matrix element usually depends weakly on energy in homogeneous semiconductors or compositional semiconductor quantum wells. In contrast, as outlined in the theoretical part of this paper, the oscillator strength increases exponentially with energy in the sawtooth superlattice. Thus, the oscillator strength has an opposite dependence on energy, as compared to the thermal distribution. Consequently, transitions via excited states can be observed in the sawtooth structure, even though they may be sparsely populated.

The photoluminescence spectrum displayed in Fig. 2 has a stronger light-hole transition ($0e \rightarrow 0\text{lh}$) as compared to the corresponding heavy-hole transition ($0e \rightarrow 0\text{hh}$). We will now proceed to explain this finding. According to Eq. (9), the oscillator strength is inversely proportional to α_f, which describes the decay of the final-state wave function in the classically forbidden region. Since α_f is proportional to $(m^*)^{1/3}$ [see Eq. (7)], the oscillator strengths of light-hole transitions are larger. In other words, because the light-hole wave function extends more into the classically forbidden region, the overlap of electron and light-hole wave functions is larger. In addition, the light-hole transition ($0e \rightarrow 0\text{lh}$) is of higher energy as compared to the corresponding heavy-hole transitions, which also contributes to the larger oscillator strength.[11]

Next, a quantitative analysis is provided to understand the shift of the quantum-confined photoluminescence transitions as a function of excitation intensity. In this analysis we assume an exponential decay of the radiative recombination. In continuous-wave photoluminescence experiments, the generation rate and recombination rate coincide, i.e.,[12]

$$\frac{dn}{dt} = \frac{n}{\tau} . \tag{10}$$

We will now show that the radiative lifetime τ can be determined from our experiments, since both the generation rate dn/dt is known at a given excitation intensity and the free-carrier concentration n can be determined from screening caused by the free carrier. To determine n we consider the shift of quantum-confined transitions in Fig. 3, which is further illustrated by the dashed line. For an increase of the excitation intensity from 2 mW (25 W/cm^2) by a factor of 10 to 20 mW (250 W/cm^2) the $0e \rightarrow 0\text{lh}$ transition, which is the strongest transition, increases in peak energy from 1.208 to 1.240 eV. We attribute this change of the peak energy to screening of dopant charge by the photogenerated carrier. The result of screening is easily illustrated by considering the photoluminescence energy given by

$$E = E_g^{\text{GaAs}} - \tfrac{1}{2} eFz_p + E_n^e + E_n^h , \tag{11}$$

where E_g^{GaAs} is the gap energy of GaAs, $\frac{1}{2}eFz_p$ is the modulation of the superlattice potential, and E_n^e and E_n^h are the electron and hole eigenstate energies. The electric field F is screened under photoexcitation and changes by an amount of

$$\Delta F = \frac{e}{2\epsilon} \Delta n_{2D} , \tag{12}$$

where n_{2D} is the excitation-induced density of carriers per quantum well. Thus, the recombination energy increases due to the reduction of potential modulation, as is evident in Eq. (11). Upon screening, the potential modulation is reduced, and the individual V-shaped quantum wells widen. The eigenstate energies of the confined states reduce accordingly. The change in eigenstate energies [which is proportional to $(\Delta n_{2D})^{2/3}$ according to Eq. (8)] is smaller than the change in potential modulation

$$\Delta E/e = \Delta F \tfrac{1}{2} z_p , \tag{13}$$

[which is proportional to Δn_{2D} according to Eq. (12)], and we therefore neglect the changes in eigenstate ener-

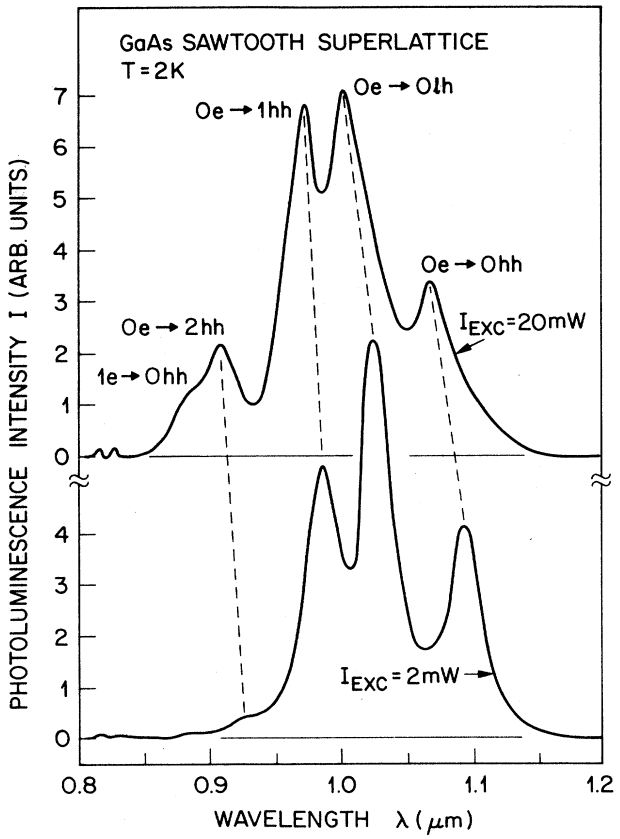

FIG. 3. Low-temperature photoluminescence spectrum of a sawtooth superlattice at two different excitation powers, 2 mW and 20 mW. The intensity of high-energy transitions (e.g., $1e \rightarrow 0$hh) increases with excitation density.

gies. Insertion of Eq. (13) into Eq. (12) allows us to determine Δn_{2D} as a function of the shift of the luminescence energy ΔE.

Finally, the generation rate can be determined from the exciting laser power P according to

$$\frac{dn}{dt} = \frac{P}{\hbar\omega} \frac{\alpha}{r^2\pi} , \tag{14}$$

where $\hbar\omega$ is the energy of exciting photons, α ($=4\times10^4$ cm^{-1}) is the absorption coefficient, and r ($=50$ μm) is the radius of the laser beam on the sample surface. The lifetime of carriers obtained from Eq. (10) using the data provided above is $\tau \cong 10$ ns at $P_L = 20$ mW. Note that the lifetime of $\tau \cong 10$ ns is an upper limit, because changes in the eigenstate energies are not taken into account. This lifetime is slightly longer compared to lifetimes in homogeneous GaAs. We attribute the increase in lifetime due to a smaller overlap of wave functions, as illustrated in Fig. 1. The photoinduced carrier density inferred from this lifetime is 4×10^{17} cm^{-3} at $P_L = 20$ mW.

Figure 3 further illustrates that high-energy transitions (e.g., $0e \rightarrow 1$hh and $0e \rightarrow 0$lh) gain intensity relative to the lowest transition. In addition, a new peak and shoulder arise at the high-energy side of the spectrum. We attribute the peak and shoulder to the $0e \rightarrow 2$hh and $1e \rightarrow 0$hh transition in agreement with absorption measurements on the same sample.[5] The occurrence of the new transitions cannot be understood solely on the basis of screening. The new, high-energy transitions can be explained by band filling or a higher effective carrier temperature at increased excitation intensity.[13]

In conclusion, we have investigated the photoluminescence characteristics of sawtooth superlattices. Multisubband quantum-confined transitions are observed and clearly resolved. We show that the oscillator strength and the thermal distributions of carriers have opposite, exponential dependences on energy. This unique feature results in the presence of several quantum-confined transitions of comparable intensity. A variational calculation is employed to obtain eigenstate energies and wave functions in an analytic form. Experimental quantum-confined transition energies are attributed to calculated energies with very good agreement. In addition, the excitation-intensity dependence of the photoluminescence spectrum is analyzed. At higher excitation densities, quantum-confined transitions shift to higher energies, and new transitions become observable. The changes of the photoluminescence spectra can be understood on the basis of screening, band filling, and increased carrier temperature at higher excitation intensity. The multisubband photoluminescence results reported here open up new possibilities for semiconductor research, such as the study of quantum effects in a periodic potential that is generated purely by dopant charges.

[1]See, for example, L. Esaki, IEEE J. Quantum Electron. **QE-22**, 1611 (1986), and other publications in this special issue on semiconductor quantum wells and superlattices.

[2]See, for example, *Heterojunction Band Discontinuities*, edited by F. Capasso and G. Margaritondo (North-Holland, New York, 1987).

[3]L. Esaki and R. Tsu, IBM J. Res. Dev. **14**, 61 (1970).

[4]E. F. Schubert, J. E. Cunningham, and W. T. Tsang, Phys. Rev. B **36**, 1348 (1987).

[5]E. F. Schubert, B. Ullrich, T. D. Harris, and J. E. Cunningham, Phys. Rev. B **38**, 8305 (1988).

[6]F. F. Fang and W. E. Howard, Phys. Rev. Lett. **16**, 797 (1966).

[7]Employment of the Wentzel-Kramers-Brillouin approximation yields identical α_n. Employment of Eq. (7) yields similar α_n with differences smaller than a factor of 2.

[8]For a review on the photoluminescence properties of *n-i-p-i* structures, see K. Ploog and G. H. Döhler, Adv. Phys. **32**, 285 (1983).

[9]Multisubband luminescence transitions in (AlGa)As/GaAs quantum wells under high excitation intensities have been reported by R. C. Miller, D. A. Kleinman, O. Munteanu, and W. T. Tsang, Appl. Phys. Lett. **39**, 1 (1981). See also G. Tränkle, A. Forchel, E. Lach, F. Scholz, M. H. Pilkuhn, G. Weimann, H. Kroemer, S. Subbanna, and G. Griffiths, *Insti-*

tute of Physics Conference Proceedings Series (IOP, Bristol, 1987), Vol. 83, p. 221. See also G. Tränkle, H. Leier, A. Forchel, H. Haug, C. Ell, and G. Weimann, Phys. Rev. Lett. **58**, 419 (87). The excitation intensites used by these groups are typically 3 orders of magnitude higher, as compared to the intensities reported here.

[10]The line shape of photoluminescence signals in semiconductors is determined by (i) thermal distribution of carriers and (ii) density of states [E. W. Williams and H. B. Bebb, in *Semiconductors and Semimetals,* edited by R. K. Willardson and A. C. Beer (Academic, New York, 1972), Vol. 8, p. 181], as well as (iii) inhomogeneous broadening mechanisms such as alloy broadening [E. F. Schubert, E. O. Göbel, Y. Horikoshi, K. Ploog, and H. J. Queisser, Phys. Rev. B **30**, 813 (1986)] or layer-thickness fluctuations [J. Hegarty and M. D. Sturge, J. Opt. Soc. Am. B **2**, 1143 (1985)].

[11]For a review, see G. H. Döhler, IEEE J. Quantum Electron. **QE-22**, 1682 (1986). See also K. Ploog and G. H. Döhler, Adv. Phys. **32**, 285 (1983).

[12]The monomolecular rate equation used here is the basis of an exponential decay of the luminescence intensity. Nonradiative-recombination processes are not considered.

[13]The explanation suggested here is based on single-valued carrier temperatures for electrons and holes. Such single carrier temperatures can be used only if the intersubband relaxation time (within the conduction or valence band) is shorter than the radiative recombination time. The radiative recombination time in sawtooth superlattices has been determined to be in the nanosecond range [see E. F. Schubert, Y. Horikoshi, and K. Ploog, Phys. Rev. B **32**, 1085 (1985)] or longer (Ref. 11), which exceeds the subnanosecond intersubband scattering time of compositional quantum wells [D. Y. Oberli, D. R. Wake, M. V. Klein, J. Klem, T. Henderson, and H. Morkoç, Phys. Rev. Lett. **59**, 696 (1987)]. Caution is required in such a comparison, because intersubband scattering times of compositional quantum wells and dopant-charge-induced quantum wells may not be identical.